Two-Level Response and Parameter Mapping Optimization for Magnetic Shielding

Guillaume Crevecoeur[1], Peter Sergeant[1], Luc Dupré[1], and Rik Van de Walle[2]

[1]Department of Electrical Energy, Systems and Automation, Ghent University, B-9000 Ghent, Belgium
[2]Department of Electronics and Information Systems, Ghent University, B-9000 Ghent, Belgium

We present a new technique for reducing computation time of numerical solutions to optimal design problems. We incorporate in the optimization procedure a coarse model. Our technique, the two-level response and parameter mapping (RPM) algorithm, is based on space mapping and manifold mapping. Space mapping (SM) performs a mapping between the parameter spaces of the coarse and fine models, while manifold mapping (MM) makes a mapping between the response spaces of the coarse and fine models through the use of response correction. Here, we use and compare the three two-level optimization procedures, SM, MM, and RPM, for the optimization of passive and active shields in induction heating. The results demonstrate accurate and time-efficient optimization of magnetic shields by the RPM algorithm.

Index Terms—**Induction heating, magnetic shielding, manifold mapping, optimization, response correction, space mapping.**

I. Introduction

THE analysis of electromagnetic phenomena in complex systems demands the use of time-consuming numerical methods. If one wants to optimize the system for certain objectives, using traditional direct optimization procedures, e.g., the Nelder–Mead simplex method, simulated annealing, genetic algorithm, etc., several computations are needed in the numerical model. As a result, the computational time for obtaining the solution of the optimization may become large. Therefore, the need exists to accelerate the optimal design procedures in engineering systems. Surrogate optimization has been used for accelerating time-consuming optimization problems [1], [2].

Two different types of surrogates can clearly be distinguished. The first type comprises approximation models which are built by fitting or interpolating response data. The response data are obtained by evaluating the model for a certain set of sample points in the design space. Response surface modeling [3], radial basis functions [4], and Kriging [5] are three frequently used approximation models. The other type of surrogate is a model which is physically based on the problem and where some simplifications or assumptions have been carried out. In electromagnetic field problems, this coarse model can be constructed by making some assumptions according to the geometry, nonlinearity, material characteristics, sources, etc. The coarse model can also be created on the basis of the numerical fine model, where some time-consuming subprocedures are not included or where a coarse discretization is used instead of a fine one.

The recently introduced efficient global optimization (EGO) algorithm by Jones *et al.* [6] for the solution of optimization problems with computationally expensive black-box functions, uses the first type of surrogates. In particular, the Kriging approximation model is employed together with expected improvement. Expected improvement is a figure of merit that balances local and global search. A probabilistic framework, the so-called no-free-lunch [7], can be used to measure the match between a specific optimization problem and its algorithm. In [8], for instance, the fit of hybrid algorithms to a particular problem is measured using the no-free-lunch framework.

The space mapping (SM) techniques, introduced by Bandler *et al.* [9], are surrogate-based optimization techniques where a coarse model is exploited and aligned with the computationally intensive fine model. The optimization routines for the original time consuming model are expanded with this coarse model: two-level optimization. The techniques have successfully been applied in the field of microwaves for component and system modeling. For a review, see [10]. The techniques were also applied for the design of a linear actuator [11] and for the design of passive shields [12]. In this paper, several two-level optimization schemes are described and compared in performance for a shielding application. In this introduction, a brief qualitative outline of these algorithms is given; in Section III, a more detailed study including mathematical background is carried out.

Traditional SM techniques try to map the parameter spaces of both the fine and the coarse model. The SM techniques might fail to converge to the optimum of the accurate model when the response space of the coarse and the response space of the fine model are severely misaligned [13].

The so-called space mapping based interpolating surrogate scheme (SMIS), introduced in [14], tackles this problem by introducing "response correction." The SMIS tries to map on the one hand the parameter spaces of both the fine and the coarse model and on the other hand the response spaces of the two models.

More recently, Koziel *et al.* described in [15] a generalized implicit space-mapping (GISM) framework that forces exact matching of responses and Jacobians between the surrogate and the fine model. The GISM and SMIS algorithm utilize a more general surrogate model but they have drawbacks. Jacobians need to be evaluated and the set of mapping parameters, which can become large, needs to be optimized using the coarse model in every step.

The manifold mapping (MM) approach, presented in [13] and applied in [16], also uses the response correction principle but moreover employs a different update scheme for the determination of the optimal parameters. The mapping parameters are obtained on the basis of the calculated responses of the coarse and fine model and do not need to be obtained through optimization.

Digital Object Identifier 10.1109/TMAG.2007.911661

Color versions of one or more of the figures in this paper are available online at http://ieeexplore.ieee.org.

The optimization problem of shielding is an interesting optimization problem because it possesses the following characteristics. When simulating the coarse and fine model responses for the passive shield only, the responses are very similar [12]. On the other hand, for the simulation of the passive and active shield, the responses are severally misaligned. Further, optimizing the active and passive shield using the coarse model is on itself hard: exhaustive search (genetic algorithm) is needed in order to obtain a global optimum. The determination of the large set of mapping parameters is consequently very hard when the SMIS and GISM algorithms are used. The determination of the Jacobians in the numerical fine model is also rather hard and very time-consuming. When utilizing the SM or the MM algorithm, one would not use a more general surrogate model as the one in the SMIS algorithm but the mapping parameters are determined in a far easier way. This shielding optimization problem has already been solved using a one-level algorithm, the genetic algorithm [17]. A global optimum was obtained, but the needed computational time for solving the optimization problem was high.

In this paper, we propose the response and parameter mapping (RPM) algorithm. The RPM algorithm performs, besides a mapping in the parameter space (as in SM), also a mapping in the response spaces (as in MM) of the fine and coarse model. The main difference between the SMIS and the GISM algorithm is the fact that a composite mapping formulation is used and that the mapping parameters are obtained on the basis of the coarse and the fine model responses. The RPM algorithm was first applied to the multiobjective optimization of the passive shield only. Further, the two-level algorithm was applied to the difficult optimization problem of the active and passive shield. Comparisons were carried out with the other two-level optimization algorithm and the one-level genetic algorithm.

II. Optimization Problem of Magnetic Shielding in Induction Heating

The chosen application example on which the optimization routines are applied, is the design of magnetic shields for an induction heating device with configuration shown in Fig. 1. The time-dependent magnetic field generated by the excitation coil of this device can treat a metallic specimen in a thermal way. The excitation coil creates also a magnetic field in the surrounding region. The operator of the equipment as well as electronic devices may be exposed to magnetic fields that are significantly higher than the reference levels of the International Commission on Non-Ionizing Radiation Protection (ICNIRP) [18] and the European Union [19], [20]. The goal of the optimization is to mitigate the magnetic field in a given area by using on the one hand passive shielding, which uses suitable materials to limit electromagnetic losses within the shield, and on the other hand active shielding, which generates counter fields opposite to the main one by proper currents in a number of compensation coils. Next to the field reduction, the optimization problem has some other objectives. For example, the modification of the thermal treatment of the work piece by the passive and active shielding must be limited to a minimum. It is obvious that the problem is a multiobjective optimization problem, where the total "cost" function $K(\cdot)$ to minimize is the weighted sum of

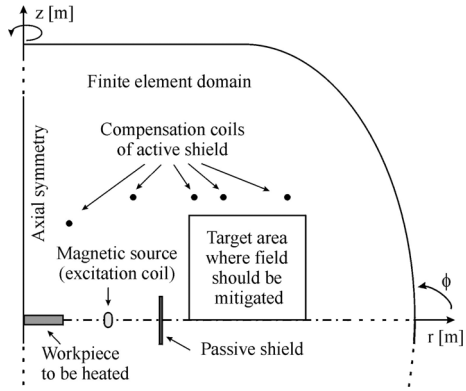

Fig. 1. Magnetic source, workpiece, passive shield, compensation coils, and target area.

the following contributions, to be determined by the fine or the coarse model:

$$K(\cdot) = w_1 B_{\text{avg}} + w_2 P_p + w_3(P_{w0} - P_w) + w_4 C_p \quad (1)$$

where

B_{avg}	average flux density in the target area with surface S_{TA}: $B_{\text{avg}} = (\int_{\text{TA}} \lvert B\rvert ds)/(S_{\text{TA}})$ where $\lvert B\rvert = \sqrt{\lvert B_r\rvert^2 + \lvert B_z\rvert^2}$ with B_r, B_z being the radial respectively the z-component of the flux density phasors in the time-harmonic, quasi-static coarse or fine model;
P_p	power dissipated in the passive shield;
$w_3(P_{w0} - P_w)$	power in the workpiece without shield P_{w0} minus the power with shield present P_w indicates the disturbing influence on the heating process;
C_p	investment cost to build the shield.

The weighting coefficients w_i determine the impact of each term on the solution. The influence of a high weighting factor w_2 (relative to w_1) in (1) results in an optimal shield with small height far from the source, in order to reduce the losses in this shield. The factor w_3 mainly influences the optimal radius. If both w_2 and w_3 are very small compared to w_1, the optimal shield is very high and very close to the source: it mitigates the field effectively, but it may dissipate much power and have a strong influence on the heating process in the work piece. The factor w_4 finally may be used to avoid geometries that are difficult to construct. Finally, the geometrical area in which to add shields is constrained, as the accessibility of the work piece should be guaranteed.

By solving the multiobjective optimization problem, the optimal position and height of the passive shield, as well as the optimal current for the active shield and the number of turns of all coils have to be returned. In order to apply space mapping, an analytical coarse model is constructed besides the fine numerical model based on the finite-element method. The fine and coarse model calculate the magnetic field distributions in the target area and the other electromagnetic quantities needed

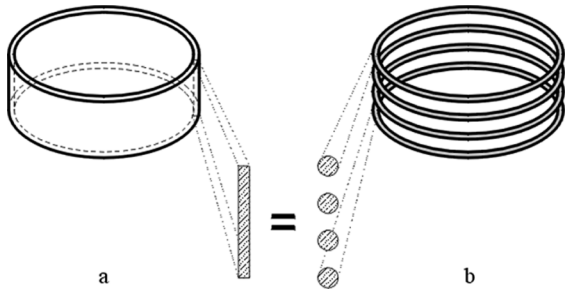

Fig. 2. The passive shield in (a) is replaced by a number of mutually coupled coils in (b). The section of the passive shield equals the sections of all equivalent coils together.

to compute (1). The optimization problem that has to be solved is given by

$$\mathbf{x}_f^* = \arg\min_{\mathbf{x}_f} K(\mathbf{f}(\mathbf{x}_f)) \tag{2}$$

with $K(\cdot)$ being the objective function (1), which calculates the "cost" of the fine model $\mathbf{f}$ of an active and/or a passive shield with the variables $\mathbf{x}_f$ as inputs.

In order to evaluate $K(\cdot)$, the *fine model* uses a time-harmonic, quasi-static finite-element model of the axisymmetric induction heater with geometry of Fig. 1. The domain is defined by the work piece, the excitation coil and the air surrounding the induction heater. The chosen shield material is copper. Details about the model as well as an experimental verification can be found in [17].

In the *coarse model*, the axisymmetric copper shield is replaced by a set of equivalent coaxial coils, see Fig. 2. Each coil has its own resistance, self inductance, and mutual inductances between the coil and all other coils. This results in an electrical circuit in which the components are calculated by well-known analytical formulas for nonferromagnetic passive shields (shielding by eddy currents) [21]. The sources in the circuit are the voltages that the excitation coil induces in the open coils of the replaced passive shield. Consequently, these voltages result from the nondistorted magnetic field, generated by the excitation coil in presence of the work piece. The induced voltages are obtained by one previous finite-element calculation of the unshielded induction heater. This voltage source representation of the induction heater stray field has the advantages that the stray field is modeled more accurately and that also ferromagnetic workpieces can be modeled, whereas the analytical expressions used in the coarse model can only take into account nonferromagnetic objects. The disadvantage is that the third term in the objective value—the change of P_w—cannot be calculated in the coarse model. Other approximations in this coarse model are the replacement of the continuous thin shield by a number of coils with discrete positions, and the uniform current distribution in the equivalent coils without taking into account possible skin effect. Consequently, the coarse model is less accurate than the fine model, but obviously, it is much faster.

III. Two-Level Optimization

A. Introduction

The m-dimensional response vector of the coarse (fine) model for a certain n-dimensional control variable vector $\mathbf{x}_c \in X_c (\mathbf{x}_f \in X_f)$, is denoted by $\mathbf{c}(\mathbf{x}_c) \in \Omega_c (\mathbf{f}(\mathbf{x}_f) \in \Omega_f)$. For the case of the optimization of magnetic shields, the control variables $\mathbf{x}$ are the height and position of the passive shield and the currents and positions of the various coils of the active shield, while the responses are the magnetic induction values in the target area and the three other terms shown in (1).

In the following sections, we alter (2) to the following:

$$\mathbf{x}_f^* = \arg\min_{\mathbf{x}_f \in X_f} \|\mathbf{f}(\mathbf{x}_f) - \mathbf{y}\|. \tag{3}$$

$\mathbf{y}$ is the objective of the optimization problem: the specifications of the aim in the optimization problem. Since we want to minimize the induction values in the target area and the other terms in (1), $\mathbf{y}$ is $\mathbf{0}$ in the case of the magnetic shields optimization. In this paper, we perform two-level optimization using space mapping (SM) techniques, the manifold mapping (MM) algorithm, and the proposed response and parameter mapping (RPM) algorithm for the magnetic shields optimization.

B. Space Mapping Techniques

The research on space mapping (SM) has expanded enormously since its introduction [10]. In space mapping, the coarse model is used as a basis for generating successive surrogates for the fine model. A suitable surrogate model is obtained by constructing a mapping between the parameter spaces of the two models. We want to generate a parameter mapping function $\mathbf{p}(\mathbf{x}_f)$ in order to obtain an approximation of the form

$$\mathbf{f}(\mathbf{x}_f) \approx \mathbf{c}(\mathbf{p}(\mathbf{x}_f)). \tag{4}$$

Finding the parameter mapping function $\mathbf{x}_c = \mathbf{p}(\mathbf{x}_f)$, the so-called parameter extraction (PE), is a very important subproblem of the SM technique [10]. The parameters of the coarse model or surrogate are extracted so that the coarse model matches the fine model:

$$\mathbf{p}(\mathbf{x}_f) = \arg\min_{\mathbf{x}_c \in X_c} \|\mathbf{c}(\mathbf{x}_c) - \mathbf{f}(\mathbf{x}_f)\| \tag{5}$$

for some specific norm.

The popular aggressive space mapping (ASM) algorithm uses the following surrogate model in the kth iteration [22]:

$$\mathbf{s}_{\mathrm{ASM}}^{(k)}(\mathbf{x}_f) = \mathbf{c}(\mathbf{p}^{(k)}(\mathbf{x}_f)) \tag{6}$$

with

$$\mathbf{p}^{(k)}(\mathbf{x}_f) = \mathbf{p}\left(\mathbf{x}_f^{(k)}\right) + \mathbf{B}^{(k)}\left(\mathbf{x}_f - \mathbf{x}_f^{(k)}\right). \tag{7}$$

$\mathbf{x}_f^{(k)}$ is the kth quasi-Newton iteration and $\mathbf{B}^{(k)}$, which is an approximation of the Jacobian of $\mathbf{p}(\mathbf{x}_f^{(k)})$, can be updated using Broyden's rank one formula [23]. The hybrid ASM algorithm (HASM) enables switching between direct optimization and the space mapping technique. For further details, see [24].

The ASM algorithm fails to converge if the coarse and the fine model are severely misaligned [13]. So-called response correction needs to be implemented. A type of space mapping that implements response correction is the space mapping based interpolating surrogate scheme (SMIS). This algorithm uses the following surrogate model $\mathbf{s}_{\mathrm{SMIS}}^{(k)}(\mathbf{x}_f)$ in the kth iteration [14]:

$$\boldsymbol{\alpha}^{(k)}\left(\mathbf{c}(\mathbf{B}^{(k)}\mathbf{x}_f + \mathbf{P}^{(k)}\right) - \mathbf{c}(\mathbf{B}^{(k)}\mathbf{x}_f^{(k)} + \mathbf{P}^{(k)})) + \boldsymbol{\beta}^{(k)} \tag{8}$$

where some specifications can be made regarding the defect correction matrix $\boldsymbol{\alpha}^{(k)}$ and vector $\boldsymbol{\beta}^{(k)}$. It is assumed that the defect correction matrix is diagonal and that $\boldsymbol{\beta}^{(k)} = \mathbf{f}(\mathbf{x}_f^{(k)})$. Response correction is applied in this algorithm and the mapping parameters $\boldsymbol{\alpha}^{(k)}, \mathbf{B}^{(k)}$, and $\mathbf{P}^{(k)}$ are identified using a parameter extraction procedure. In the generalized implicit space mapping framework (GISM), their mapping parameters need to be identified in a similar way [15].

We emphasize that in every iteration of the SM method, only *one evaluation of the fine model* ($\mathbf{f}(\mathbf{x}_f^{(k)})$) and *one solution of a minimization in the coarse model* (5) are carried out.

C. Manifold Mapping Techniques

Besides the SM approach, where a mapping has to be determined in the parameter space only, there exists a manifold mapping (MM) approach, where an affine mapping is defined in the response space only. An affine map between two vector spaces consists of a linear transformation followed by a translation. The manifold mapping uses the following surrogate model in the kth iteration [16]:

$$\mathbf{s}_{\mathrm{MM}}^{(k)}(\mathbf{x}_f) = \mathbf{f}\left(\mathbf{x}_f^{(k)}\right) + \mathbf{D}^{(k)}(\mathbf{c}(\mathbf{x}_f) - \mathbf{c}\left(\mathbf{x}_f^{(k)}\right)) \tag{9}$$

where $\mathbf{D}^{(k)}$ is a regular $m \times m$ matrix. The iteration $\mathbf{x}_f^{(k+1)}$ is computed the following way:

$$\mathbf{x}_f^{(k+1)} = \arg \min_{\mathbf{x}_f \in X_c} \|\mathbf{s}_{\mathrm{MM}}^{(k)}(\mathbf{x}_f) - \mathbf{y}\|. \tag{10}$$

$\mathbf{x}_c = \mathbf{x}_f$ in the MM algorithm. The algorithm has been successfully applied to the design of a linear actuator [16]. The surrogate model (9) is similar to the surrogate model (8). The main difference between the SMIS algorithm and the MM algorithm is the use of different update schemes. The $\mathbf{D}^{(k)}$-matrices are evaluated using the responses in the fine and coarse models in the previous iterations, while the SMIS algorithm uses the parameter extraction procedure. For a detailed description, see [13].

We underline again that in every iteration of the MM method, only *one evaluation of the fine model* ($\mathbf{f}(\mathbf{x}_f^{(k)})$) and *one solution of a minimization in the coarse model* (10) are carried out.

D. Response and Parameter Mapping

The response and parameter mapping (RPM) algorithm is based on the SM and the MM approach. The algorithm is based on the space mapping approach, due to the use of a parameter mapping function between the parameter spaces of the coarse and fine model. The RPM algorithm is also based on the response correction principle by establishing a surrogate model with an affine mapping in the response spaces of the coarse and fine model. The RPM algorithm employs an affine mapping between the response spaces of the coarse and fine model and employs an affine mapping between the parameter spaces of the two models.

The RPM algorithm is built in the following way, by using the surrogate model:

$$\mathbf{s}_{\mathrm{RPM}}(\mathbf{x}) = \mathbf{S}(\mathbf{c}(\mathbf{p}(\mathbf{x}))) \tag{11}$$

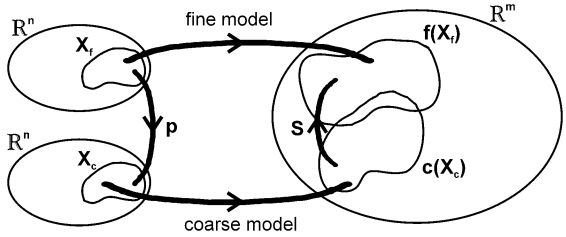

Fig. 3. Diagram of the mappings performed in the RPM method. The time-consuming evaluation in the fine model $\mathbf{f}(\mathbf{x}_f)$ is replaced by the surrogate model $\mathbf{s}(\mathbf{x}_f) = \mathbf{S}(\mathbf{c}(\mathbf{p}(\mathbf{x}_f)))$.

with response mapping function $\mathbf{S}$ and parameter mapping function $\mathbf{p}$. Fig. 3 shows a diagram of the mappings performed in the RPM algorithm. The space mapping algorithm employs only the $\mathbf{p}$-mapping (with $\mathbf{S}$ the identity mapping), whereas the manifold mapping algorithm employs only the $\mathbf{S}$-mapping (with $\mathbf{p}$ the identity mapping or a certain constant mapping). The RPM replaces the time expensive evaluation in the fine model $\mathbf{f}(\mathbf{x}_f)$ by employing the surrogate (11). In this section, we denote $\mathbf{x} = \mathbf{x}_f$ to simplify the notation. The goal is to obtain the optimal parameters $\mathbf{x}^*$ with $\hat{\mathbf{S}}$ and $\hat{\mathbf{p}}$ being the correctly recovered mapping functions:

$$\hat{\mathbf{S}}(\mathbf{c}(\hat{\mathbf{p}}(\mathbf{x}^*))) = \mathbf{f}(\mathbf{x}^*). \tag{12}$$

We denote $\mathbf{S}$ as the response mapping function and we denote $\mathbf{p}$ as the parameter mapping function. We propose to build up the mapping in the following way:

$$\mathbf{S}(\mathbf{c}(\mathbf{p}(\mathbf{x}))) = \mathbf{f}(\mathbf{x}^*) + \mathbf{D}(\mathbf{c}(\mathbf{p}(\mathbf{x})) - \mathbf{c}(\mathbf{p}(\mathbf{x}^*))). \tag{13}$$

This mapping is similar to (8). When performing this mapping in an iterative way, we have the following iterative surrogate model $\mathbf{S}^{(k)}(\mathbf{c}(\mathbf{p}^{(k)}(\mathbf{x})))$:

$$\mathbf{f}(\mathbf{x}^{(k)}) + \mathbf{D}^{(k)}(\mathbf{c}(\mathbf{p}^{(k)}(\mathbf{x})) - \mathbf{c}(\mathbf{p}^{(k)}(\mathbf{x}^{(k)}))). \tag{14}$$

For the definition of the parameter mapping function $\mathbf{p}^{(k)}$ in the kth iteration, we start from the following aim:

$$\mathbf{p}(\mathbf{x}^*) = \widetilde{\mathbf{x}}^* \tag{15}$$

with

$$\widetilde{\mathbf{x}}^* = \arg \min_{\mathbf{x}} \|\mathbf{c}(\mathbf{x}) - \mathbf{f}(\mathbf{x}^*)\|. \tag{16}$$

We propose the following affine mapping in the parameter space in the kth iteration

$$\mathbf{p}^{(k)}(\mathbf{x}) = \widetilde{\mathbf{x}}^{(k)} + \mathbf{B}^{(k)}(\mathbf{x} - \mathbf{x}^{(k)}) \tag{17}$$

where the parameter value $\widetilde{\mathbf{x}}^{(k)}$ is defined as follows:

$$\widetilde{\mathbf{x}}^{(k)} = \arg \min_{\mathbf{x}} \|\mathbf{c}(\mathbf{x}) - \mathbf{f}(\mathbf{x}^{(k)})\|. \tag{18}$$

We remark that (17) and (18) are similar to (7) and PE-step (5).

Finally, $\mathbf{S}^{(k)}(\mathbf{c}(\mathbf{p}^{(k)}(\mathbf{x})))$ is given by

$$\mathbf{f}(\mathbf{x}^{(k)}) + \mathbf{D}^{(k)}(\mathbf{c}(\widetilde{\mathbf{x}}^{(k)} + \mathbf{B}^{(k)}(\mathbf{x} - \mathbf{x}^{(k)})) - \mathbf{c}(\widetilde{\mathbf{x}}^{(k)})) \tag{19}$$

where the update of $\mathbf{D}^{(k)}$ and $\mathbf{B}^{(k)}$ are performed in a similar way as the MM approach. In the algorithm, we use thus two different iteration schemes $\mathbf{x}^{(k)}$ and $\widetilde{\mathbf{x}}^{(k)}$, where $\mathbf{x}^{(k)}$ are the recovered iterations of the response mapping and the parameter mapping and $\widetilde{\mathbf{x}}^{(k)}$ are the iterations obtained from the parameter mapping only.

The main iteration scheme of the RPM algorithm is given by

1) Set $k=0$, $\mathbf{B}^{(0)}=\mathbf{I}$, and $\mathbf{D}^{(0)}=\mathbf{I}$ and compute
$$\mathbf{x}^{(0)}=\arg\min_{\mathbf{x}}\|\mathbf{c}(\mathbf{x})-\mathbf{y}\|. \tag{20}$$
2) Evaluate $\mathbf{x}^{(k)}$ in the fine model: $\mathbf{f}(\mathbf{x}^{(k)})$.
3) Compute $\widetilde{\mathbf{x}}^{(k)}=\mathbf{p}^{(k)}(\mathbf{x}^{(k)})$
$$\widetilde{\mathbf{x}}^{(k)}=\arg\min_{\mathbf{x}}\|\mathbf{c}(\mathbf{x})-\mathbf{f}(\mathbf{x}^{(k)})\| \tag{21}$$
and evaluate $\mathbf{c}(\widetilde{\mathbf{x}}^{(k)})$. If $k=0$, then $\widetilde{\mathbf{x}}^{(0)}=\mathbf{x}^{(0)}$.
4) If $k>0$, then build the following parameter mapping function:
$$\mathbf{p}^{(k)}(\mathbf{x})=\widetilde{\mathbf{x}}^{(k)}+\mathbf{B}^{(k)}(\mathbf{x}-\mathbf{x}^{(k)}). \tag{22}$$
Compute $\mathbf{B}^{(k)}$ in the following way, see also [13]:
$$\mathbf{B}^{(k)}=\Delta\widetilde{\mathbf{X}}\Delta\mathbf{X}^{\dagger}+\left(\mathbf{I}-\mathbf{U}_{\widetilde{x}}\mathbf{U}_{\widetilde{x}}^{T}\right)\left(\mathbf{I}-\mathbf{U}_{x}\mathbf{U}_{x}^{T}\right) \tag{23}$$
with the columns of $\Delta\mathbf{X}$ and $\Delta\widetilde{\mathbf{X}}$ respectively given by $\Delta\mathbf{X}_i=\mathbf{x}^{(k-i)}-\mathbf{x}^{(k)}$ and $\Delta\widetilde{\mathbf{X}}_i=\widetilde{\mathbf{x}}^{(k-i)}-\widetilde{\mathbf{x}}^{(k)}$, for $i=1,\ldots,\min(m,k)$. Their singular value decompositions are respectively $\Delta\mathbf{X}=\mathbf{U}_x\mathbf{\Sigma}_x\mathbf{U}_x^T$ and $\Delta\widetilde{\mathbf{X}}=\mathbf{U}_{\widetilde{x}}\mathbf{\Sigma}_{\widetilde{x}}\mathbf{U}_{\widetilde{x}}^T$. For $k=0$, is the mapping function identity $\mathbf{p}^{(0)}(\mathbf{x})=\mathbf{x}$.
5) Compute $\mathbf{c}(\mathbf{p}^{(k)}(\mathbf{x}^{(k-i)}))$ for $i=1,\ldots,\min(n,k)$.
6) If $k>0$, build the following response mapping function:
$$\begin{aligned}\mathbf{S}^{(k)}(\mathbf{c}(\mathbf{p}^{(k)}(\mathbf{x})))=&\,\mathbf{f}(\mathbf{x}^{(k)})\\&+\mathbf{D}^{(k)}(\mathbf{c}(\mathbf{p}^{(k)}(\mathbf{x}))-\mathbf{c}(\mathbf{p}^{(k)}(\mathbf{x}^{(k)})))\end{aligned} \tag{24}$$
where $\mathbf{D}^{(k)}$ is computed as [13]
$$\mathbf{D}^{(k)}=\Delta\mathbf{F}\Delta\mathbf{C}^{\dagger}+(\mathbf{I}-\mathbf{U}_f\mathbf{U}_f^T)(\mathbf{I}-\mathbf{U}_x\mathbf{U}_x^T) \tag{25}$$
with the columns of $\Delta\mathbf{F}$ and $\Delta\mathbf{C}$ respectively given by $\Delta\mathbf{F}_i=\mathbf{f}(\mathbf{x}^{(k-i)})-\mathbf{f}(\mathbf{x}^{(k)})$ and $\Delta\mathbf{C}_i=\mathbf{c}(\mathbf{p}^{(k)}(\mathbf{x}^{(k-i)}))-\mathbf{c}(\widetilde{\mathbf{x}}^{(k)})$, for $i=1,\ldots,\min(n,k)$. Their singular value decompositions are respectively $\Delta\mathbf{F}=\mathbf{U}_f\mathbf{\Sigma}_f\mathbf{U}_f^T$ and $\Delta\mathbf{C}=\mathbf{U}_c\mathbf{\Sigma}_c\mathbf{U}_c^T$. For $k=0$, is $\mathbf{S}^{(0)}(\mathbf{c}(\mathbf{p}^{(0)}(\mathbf{x})))=\mathbf{f}(\mathbf{x}^{(0)})+\mathbf{c}(\mathbf{p}^{(0)}(\mathbf{x}))-\mathbf{c}(\widetilde{\mathbf{x}}^{(0)})$.
7) The next iterand is computed as
$$\mathbf{x}^{(k+1)}=\arg\min_{\mathbf{x}}\|\mathbf{S}^{(k)}(\mathbf{c}(\mathbf{p}^{(k)}(\mathbf{x})))-\mathbf{y}\| \tag{26}$$
$$\begin{aligned}&=\arg\min_{\mathbf{x}}\|\mathbf{D}^{(k)}(\mathbf{c}(\mathbf{p}^{(k)}(\mathbf{x}))\\&\quad-\mathbf{c}(\widetilde{\mathbf{x}}^{(k)}))+\mathbf{f}(\mathbf{x}^{(k)})-\mathbf{y}\|\end{aligned} \tag{27}$$
or as
$$\mathbf{x}^{(k+1)}=\arg\min_{\mathbf{x}}\|\mathbf{c}(\mathbf{p}^{(k)}(\mathbf{x}))-\mathbf{y}^{(k)}\| \tag{28}$$
with $\mathbf{y}^{(k)}=\mathbf{c}(\widetilde{\mathbf{x}}^{(k)})-[\Delta\mathbf{C}\Delta\mathbf{F}^{\dagger}+\mathbf{I}-\mathbf{U}_c\mathbf{U}_c^T](\mathbf{f}(\mathbf{x}^{(k)})-\mathbf{y})$. Equations (26) and (28) are asymptotically equivalent.
8) Set $k=k+1$, and go to step 2.

The main differences between the manifold mapping algorithm and the proposed algorithm are the construction of the parameter mapping function and the use of the $\widetilde{\mathbf{x}}^{(k)}$ iterations. This means the introduction of steps 3, 4, and 5 and the change in the computation of $\mathbf{D}^{(k)}$ and $\mathbf{x}^{(k+1)}$.

In every iteration of the RPM method, only *one evaluation of the fine model* (step 2 of the algorithm) and *two solutions of a minimization in the coarse model* [(21) and (26)] are carried out.

TABLE I
OPTIMAL PARAMETERS OF PASSIVE SHIELD

Parameters:	r_p (m)	$t_p(m)$	$h_p(mm)$	K(**x**)	No. **f** evals.
$\mathbf{x}^*_{ASM}$	0.31	0.52	0.20	217.6	4
$\mathbf{x}^*_{HASM}$	0.29	0.48	0.20	216.1	10
$\mathbf{x}^*_{MM}$	0.29	0.48	0.20	216.1	6
$\mathbf{x}^*_{RPM}$	0.29	0.48	0.20	216.1	6

IV. RESULTS FOR THE OPTIMIZATION OF ACTIVE AND PASSIVE MAGNETIC SHIELDS

For the excitation current, a sinusoidal excitation current as high as 4 kA at 1 kHz is used in the simulation, which is necessary to heat the workpiece quickly [17]. The optimization in the coarse model was performed using the genetic algorithm. For the ASM algorithm this is the evaluation of (5), for the MM algorithm this is the evaluation of expression (10) and for the RPM algorithm this is the evaluation of expressions (21) and (26). The specifications, i.e., the weighting coefficients w_i, of the cost function $K(\cdot)$ when optimizing the passive shields are given in [12] and when optimizing the passive and active shield are given in [17]. The computational effort is given by a time measure on a 2.4-GHz PC configuration.

A. Optimization Using SM

The aggressive space mapping optimization of the passive shield only was performed in [17]. Only three variables were optimized, namely the radial position r_p, thickness t_p, and height h_p of the passive shield. The obtained optimal values $\mathbf{x}^*_{\mathrm{ASM}}$ are shown in Table I. When we applied the hybrid aggressive space mapping method to the optimization problem, we obtained a solution with a lower cost evaluation. More fine model evaluations were needed for solving the problem. We applied the gradient-method as direct optimization method in the fine model. However, when applying ASM for the optimization of active and passive shields, where eight additional active shield parameters have to be determined, bad convergence properties are obtained. Fig. 4 shows the convergence history of the ASM method. The figure depicts the cost of the fine model response in every iteration $K(\mathbf{f}(\mathbf{x}_f^{(i)}))$. The fine model is only evaluated once in each iteration, namely during the evaluation of (5). We observe a low reduction in cost at the end of the optimization process compared to the cost $K(\mathbf{f}(\mathbf{x}_c^*))$ evaluated in the first

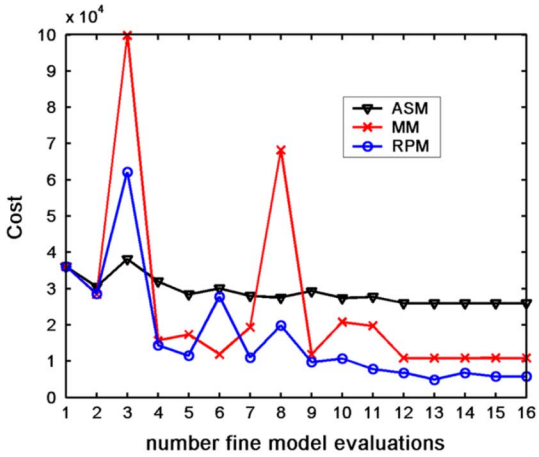

Fig. 4. Convergence history of the ASM, RPM, and MM algorithm when optimizing the active and passive shields. Here, the cost function $K(\cdot)$ of (1) is considered.

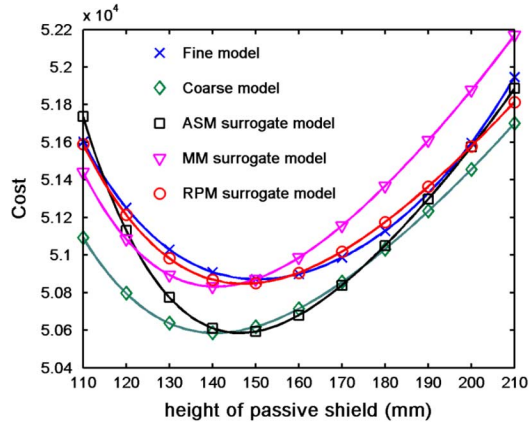

Fig. 5. Fine model, coarse model, and final surrogate models generated by ASM, MM, and RPM algorithm. Model responses generated for one variable parameter: height of passive shield, the other parameters are kept constant.

iteration. Table III shows the relative large cost $K(\mathbf{x}^*_{\mathrm{ASM}})$ obtained through ASM compared to the cost obtained through the one-level genetic algorithm.

The ASM algorithm has difficulty to converge to the optimal values, due to the fact that the objective $\mathbf{y}$ is not reachable. Indeed, ASM recovers $\overline{\mathbf{x}}_f$ from [22]:

$$\arg\min_{\mathbf{x}_c \in X_c} \|\mathbf{c}(\mathbf{x}_c) - \mathbf{f}(\mathbf{x}_f)\| = \arg\min_{\mathbf{x}_c \in X_c} \|\mathbf{c}(\mathbf{x}_c) - \mathbf{y}\| \quad (29)$$

and where it is necessary that there exists a certain $\mathbf{x}_f$ where $\mathbf{f}(\mathbf{x}_f) = \mathbf{y}$, for having good convergence properties [13]. When we added to the objective $\mathbf{y}$ a certain value ε, we obtained better optimal solutions. Nevertheless, this is not a suitable way to solve the problem, because it is never known in advance how large ε must be chosen.

Fig. 5 shows the cost function evaluations of the forward fine and coarse models and of the surrogate models. This is a cross section of the cost function surface which makes it possible to visualize the responses of the several models. The surrogate model has to approximate the fine model in the best possible way. The height of the passive shield is varying while the other parameter are kept constant. The cost of the optimal value of the surrogate model is at the same height as the cost of the optimal

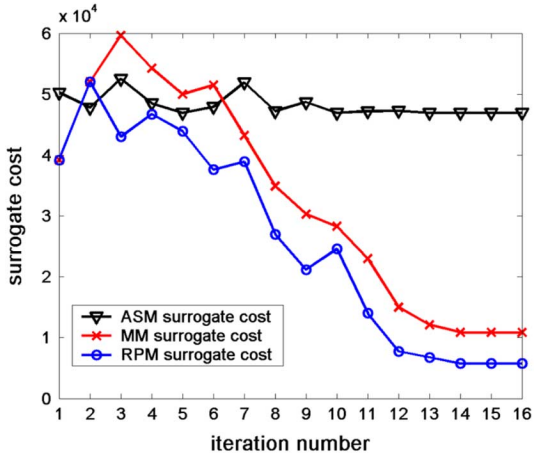

Fig. 6. Surrogate cost of ASM algorithm: $K(\mathbf{c}(\mathbf{p}^{(k)}(\mathbf{x}_f^{(k)})))$, surrogate cost of MM algorithm: $K(\mathbf{s}^{(k)}_{\mathrm{MM}}(\mathbf{x}_f^{(k+1)}))$ and surrogate cost of RPM algorithm: $K(\mathbf{s}^{(k)}_{\mathrm{RPM}}(\mathbf{x}_f^{(k+1)}))$ in every iteration. Here, the cost function $K(\cdot)$ of (1) is considered.

value of the coarse model. The space mapping method makes it not possible to change the response of the surrogate model, so that the surrogate model comes closer to the fine model. On the other hand, the figure shows that the surrogate model is closer to the fine model than that the coarse model is to the fine model.

Fig. 6 depicts the cost of the surrogate function $K(\mathbf{s}^{(k)}_{\mathrm{ASM}}(\mathbf{x}_f^{(k)})) = K(\mathbf{c}(\mathbf{p}^{(k)}(\mathbf{x}_f^{(k)})))$ in every iteration. We observe that the cost does not go below a certain value. This is due to the fact that ASM does not apply response correction, so that the surrogate model $\mathbf{s}^{(k)}_{\mathrm{ASM}}(\mathbf{x}_f^{(k)}) \neq \mathbf{f}(\mathbf{x}_f^{(k)})$ can not be corrected in every iteration. The obtained optimal value of the ASM surrogate model is not close to the optimal value of the fine model, due to the fact that the approximation of the surrogate model to the fine model is not close enough.

When we applied the SMIS algorithm to the optimization problem, problems occurred regarding the identification of the mapping parameters $\boldsymbol{\alpha}^{(k)}, \mathbf{B}^{(k)}, \mathbf{P}^{(k)}$. The large set of mapping parameters was hard to find. We applied the surface fitting parameter extraction approach, presented in [14], for the identification of the parameters. This procedure needs the evaluation of the calculated Jacobian matrices in the fine model. Applying this procedure turned out to be very time-consuming in the case of optimization of magnetic shielding. Further, nonuniqueness problems occurred for the identification of the mapping parameters. The same was observed when applying the GISM algorithm.

B. Optimization Using MM

When applying MM to the optimization problem of active and passive shielding, better convergence properties are yielded. This is shown in Fig. 4. Table II shows the needed CPU-time for the optimization of the passive shield. The implementation of the two-level algorithm yields a huge decrease in needed computational time. Response correction is not really needed in the case of passive shielding. However, when more parameters need to be optimized, response correction is needed. The MM surrogate model is a far better approximation of the fine model than the ASM surrogate model. Fig. 5 shows this graphically. The computational time needed was (approximately 10 times) more

TABLE II
NEEDED CPU-TIME FOR OPTIMIZING THE PASSIVE SHIELD ONLY

	CPU-time
Genetic Algorithm	$\approx 2\,h$
ASM	14 min
MM	19 min
RPM	26 min

TABLE III
NEEDED CPU-TIME AND COST FOR OPTIMIZING THE ACTIVE AND PASSIVE SHIELD

	CPU-time	K(**x**)
Genetic Algorithm	170 h	$5 \cdot 10^3$
ASM	16 h	$26 \cdot 10^3$
MM	17 h	$11 \cdot 10^3$
RPM	23 h	$5.7 \cdot 10^3$

computationally efficient in comparison with the genetic algorithm. See Table III for a comparison of the computational cost and the final cost $K(\cdot)$ between the several algorithms.

It was necessary to perform regularization during the MM optimization procedure for $\Delta\mathbf{F}$, so that the response mapping was stabilized. Indeed, in some iterations, $\mathbf{y}^{(k)}$-values became negative and the $|B|$-values of the surrogate response vectors have to be positive. We applied the technique proposed in [13], where $\Delta\mathbf{F}^{\dagger} = \mathbf{U}_f\mathbf{\Sigma}_f^{\dagger}\mathbf{U}_f^T$ is replaced by $\Delta\mathbf{F}_{\text{reg}}^{\dagger} = \mathbf{U}_f(\mathbf{\Sigma}_f^{\dagger} + \lambda\sigma_{\Delta F}\mathbf{I})\mathbf{U}_f^T$ $\cdot\,\sigma_{\Delta F}$ is the largest singular value of $\Delta\mathbf{F}$ and $0 \leq \lambda \leq 1$ is a trust region parameter. The optimal design resulting from this algorithm was not the same as the one resulting from the genetic algorithm and we observed a higher cost.

Fig. 6 shows that the cost of the surrogate model $K(\mathbf{s}_{\text{MM}}^{(k)}(\mathbf{x}_f^{(k+1)}))$, when evaluating (10) in every iteration, goes far below the cost of the surrogate model of the ASM algorithm. This is due to the implementation of the response correction, which implies $\mathbf{s}_{\text{MM}}^{(k)}(\mathbf{x}_f^{(k)}) = \mathbf{f}(\mathbf{x}_f^{(k)})$.

C. Optimization Using RPM

The parameter mapping in the RPM algorithm, takes simultaneously place with the response mapping. The algorithm applies a response mapping and parameter mapping where the several mapping parameters do not have to be evaluated using the difficult parameter extraction step.

Table I shows that the same optimal values are obtained as the ones obtained from the HASM and MM algorithm, when solving the optimization problem of the passive shield only. We remark that more coarse model evaluations are needed in the RPM algorithm due to the fact that steps 3 and 5 of the algorithm need additional coarse model evaluations compared to the MM algorithm. Table II shows that more computational time is needed for solving the optimization problem using the RPM algorithm. This is due to the fact that in every iteration two solutions of a minimization in the coarse model are needed while the SM and MM algorithm only need one optimization in the coarse model.

Fig. 4 illustrates the convergence history for the optimization of active and passive shields. The computational time needed was larger than the MM algorithm (about 1.4 times larger, see Table III), due to the additional optimizations in the coarse model. A lower cost was obtained at the end of the optimization, compared to the MM algorithm and the result was close to the optimal values resulting from the genetic algorithm. However, it is difficult to prove that the RPM algorithm recovers a global optimum for any test case. Indeed, in case that the coarse model is too coarse, the convergence may be questionable. Further research should be concentrated on that issue.

We have the following remarks regarding the implementation of the RPM algorithm. A regularization was performed for $\Delta\widetilde{\mathbf{X}}$ in order to stabilize the parameter mapping. Indeed, $\Delta\widetilde{\mathbf{X}}^{\dagger} = \mathbf{U}_{\widetilde{x}}\mathbf{\Sigma}_{\widetilde{x}}^{\dagger}\mathbf{U}_{\widetilde{x}}^T$ was replaced by $\Delta\widetilde{\mathbf{X}}_{\text{reg}}^{\dagger} = \mathbf{U}_{\widetilde{x}}(\mathbf{\Sigma}_{\widetilde{x}}^{\dagger} + \lambda\sigma_{\widetilde{x}}\mathbf{I})\mathbf{U}_{\widetilde{x}}^T$ where $\sigma_{\widetilde{x}}$ is the largest singular value of $\Delta\widetilde{\mathbf{X}}$. The trust region parameter λ is important for letting $\mathbf{p}^{(k)}(\mathbf{x}) \in X_c$. A regularization was also performed on the fine model space as we applied it in the MM algorithm.

Fig. 6 shows the cost of the surrogate model $K(\mathbf{s}_{\text{RPM}}^{(k)}(\mathbf{x}_f^{(k+1)}))$ when evaluating (26) in every iteration. It is shown that $\mathbf{s}_{\text{RPM}}$ goes faster to the optimal cost, compared to the $\mathbf{s}_{\text{MM}}$ model. This is due to the fact that $\mathbf{s}_{\text{RPM}}(\mathbf{x}_f)$ approximates $\mathbf{f}(\mathbf{x}_f)$ in a better way, as graphically shown on Fig. 5, than that $\mathbf{s}_{\text{MM}}(\mathbf{x}_f)$ approximates $\mathbf{f}(\mathbf{x}_f)$.

The SM and MM algorithm, which is working properly for the passive shield optimization, works also for the RPM algorithm although more CPU-time is needed when using the RPM algorithm. The passive and active optimization using the MM algorithm is working rather good but is working better using the RPM algorithm. This is due to the fact that the coarse and fine model are severally misaligned and a more general surrogate model is needed, as illustrated by Figs. 5 and 6. The RPM algorithm is suitable for optimization problems where the coarse and fine model differ importantly.

V. CONCLUSION

We optimized active and passive shields using two-level optimization methods. We applied space mapping, manifold mapping, and the novel response and parameter mapping onto the optimization problem. Good convergence properties were observed regarding the RPM algorithm, particularly due to the fact that the generated surrogate model approximates in a much better way the fine model than the surrogate models of the ASM and MM algorithm.

ACKNOWLEDGMENT

P. Sergeant is a postdoctoral researcher for the "Fonds voor Wetenschappelijk Onderzoek Vlaanderen" (FWO). This work was supported by FWO projects G.0322.04 and G.0082.06 and by the "Bijzonder Onderzoeksfonds" (BOF) of Ghent University.

REFERENCES

[1] J. E. Dennis and V. Torczon, "Managing approximate models in optimization," in *Multidisciplinary Design Optimization: State-Of-The-Art*, N. M. Alexandrov and M. Y. Hussaini, Eds. Philadelphia, PA: SIAM, 1997, pp. 330–347.

[2] A. J. Booker, J. E. Dennis Jr., P. D. Frank, D. B. Serafini, V. Torczon, and M. W. Trosset, "A rigorous framework for optimization of expensive functions by surrogates," *Struct. Optim.*, vol. 17, no. 1, pp. 1–13, Feb. 1999.
[3] D. Dyck, D. A. Lowther, Z. Malik, R. Spence, and J. Nelder, "Response surface models of electromagnetic devices and their application to design," *IEEE Trans. Magn.*, vol. 34, no. 3, pp. 1821–1824, May 1999.
[4] M.J. D. Powell, "Radial basis functions for multivariable interpolation: A review," in *Algorithms For Approximation*. Oxford, U.K.: Oxford Univ. Press, 1987.
[5] L. Lebensztajn, C. A. R. Maretto, M. C. Costa, and J.-L. Coulomb, "Kriging: A useful tool for electromagnetic device optimization," *IEEE Trans. Magn.*, vol. 40, no. 2, pp. 1196–1199, Mar. 2004.
[6] D. R. Jones, M. Schonlau, and W. J. Welch, "Efficient global optimization of expensive black-box functions," *J. Global Optim.*, vol. 13, pp. 445–492, 1998.
[7] D. Wolpert and W. Macready, "No free lunch theorems for optimization," *IEEE Trans. Evol. Comput.*, vol. 1, no. 1, pp. 67–82, Apr. 1997.
[8] O. Quevedo-Teruel, E. Rajo-Iglesias, and A. Oropesa-Garcia, "Hybrid algorithms for electromagnetic problems and the no-free-lunch framework," *IEEE Trans. Antennas Propag.*, vol. 55, no. 3, pp. 742–749, Mar. 2007.
[9] J. W. Bandler, R. M. Biernacki, S. H. Chen, P. A. Grobelny, and R. H. Hemmers, "Space mapping technique for electromagnetic optimization," *IEEE Trans. Microw. Theory Tech.*, vol. 42, no. 12, pp. 2536–2544, Dec. 1994.
[10] J. Bandler, Q. Cheng, S. Dakroury, A. Mohamed, M. Bakr, K. Madsen, and J. Søndergaard, "Space mapping: The state of the art," *IEEE Trans. Microw. Theory Tech.*, vol. 52, no. 1, pp. 337–361, Jan. 2004.
[11] D. Echeverria, D. Lahaye, L. Encica, and P. W. Hemker, "Optimization in electromagnetics with the space-mapping technique," *COMPEL-Int. J. Comput. Math. Electr. Electron. Eng.*, vol. 24, no. 3, pp. 952–966, 2005.
[12] P. Sergeant, L. Dupré, and J. Melkebeek, "Space mapping method for the design of passive shields," *J. Appl. Phys.*, vol. 99, no. 8, Apr. 2007.
[13] D. Echeverría and P. Hemker, "Space mapping and defect correction," *Comput. Methods Appl. Math.*, vol. 5, no. 1, pp. 107–136, 2005.
[14] J. Bandler, D. Hailu, K. Madsen, and F. Pedersen, "A space-mapping interpolating surrogate algorithm for highly optimized EM-based design of microwave devices," *IEEE Trans. Microw. Theory Tech.*, vol. 52, no. 11, pp. 2593–2600, Nov. 2004.
[15] S. Koziel, J. W. Bandler, and K. Madsen, "A space-mapping framework for engineering optimization—theory and implementation," *IEEE Trans. Microw. Theory Tech.*, vol. 54, no. 10, pp. 3721–3730, Oct. 2007.
[16] D. Echeverría, D. Lahaye, L. Encica, E. Lomonova, P. Hemker, and A. Vandenput, "Manifold-mapping optimization applied to linear actuator design," *IEEE Trans. Magn.*, vol. 42, no. 4, pp. 1183–1186, Apr. 2007.
[17] P. Sergeant, L. Dupré, M. De Wulf, and J. Melkebeek, "Optimizing active and passive magnetic shields in induction heating by a genetic algorithm," *IEEE Trans. Magn.*, vol. 39, no. 6, pp. 3486–3496, Nov. 2003.
[18] ICNIRP Guidelines, "Guidelines for limiting exposure to time-varying electric, magnetic, and electromagnetic fields (up to 300 GHz)," *Health Phys.*, vol. 74, pp. 494–522, Apr. 1998.
[19] European Council, "Council recommendation 1999/519/EC of 12 July 1999 on the limitation of exposure of the general public to electromagnetic fields (0 Hz to 300 GHz)," *Official Journal of the European Union*, vol. L199, pp. 59–70, Jul. 1999.
[20] European Council, "Corrigendum to directive 2004/40/EC of the European parliament and of the council of 29 Apr. 2004 on the minimum health and safety requirements regarding the exposure of workers to the risks arising from physical agents (electromagnetic fields)," *Official Journal of the European Union*, vol. L184, pp. 1–9, May 2004.
[21] E. B. Rosa and L. Cohen, Formulæ and tables for the calculation of mutual and self-inductance" Government Printing office, Washington, DC, 1908.
[22] J. W. Bandler, R. M. Biernacki, S. H. Chen, R. H. Hemmers, and K. Madsen, "Electromagnetic optimization exploiting aggressive space mapping," *IEEE Trans. Microw. Theory Tech.*, vol. 43, no. 12, pp. 2874–2882, Dec. 1995.
[23] C. G. Broyden, "A class of methods for solving nonlinear simultaneous equations," *Math. Comput.*, vol. 19, no. 92, pp. 577–593, Oct. 1965.
[24] M. H. Bakr, J. W. Bandler, N. K. Georgieva, and K. Madsen, "A hybrid aggressive space-mapping algorithm for EM optimization," *IEEE Trans. Microw. Theory Tech.*, vol. 47, no. 12, pp. 2440–2449, Dec. 1999.

Manuscript received January 25, 2007; revised October 29, 2007. Corresponding author: G. Crevecoeur (e-mail: Guillaume.Crevecoeur@ugent.be).

Guillaume Crevecoeur (S'07) was born in 1981. He received the physical engineering degree from Ghent University, Ghent, Belgium, in 2004.

He joined the Department of Electrical Energy, Systems and Automation, Ghent University, in 2004 as a doctoral student of the Special Research Fund (B.O.F.). His main research interests are numerical methods in electromagnetics and the solution of inverse problems in electromagnetics for magnetic material characterization, source localization, and geometrical optimization.

Peter Sergeant was born in 1978. He graduated in electrical and mechanical engineering in 2001 and received the degree of Doctor in engineering sciences in 2006, both from from Ghent University, Ghent, Belgium.

He joined the Department of Electrical Energy, Systems and Automation, Ghent University, in 2001 as Research Assistant. Since 2006, he has been a postdoctoral Researcher for the Fund of Scientific Research Flanders (FWO). His main research interests are numerical methods in combination with optimization techniques to design nonlinear electromagnetic systems, in particular actuators and magnetic shields.

Luc Dupré (M'01) was born in 1966. He graduated in electrical and mechanical engineering in 1989 and received the degree of Doctor in Applied Sciences in 1995, both from the Ghent University, Ghent, Belgium.

He joined the Department of Electrical Power Engineering, Ghent University, in 1989 as a Research Assistant. In 1996, he became a postdoctoral Researcher for the Fund of Scientific Research-Flanders (FWO). Since, 2002 he has been a Professor at the Engineering Faculty of Ghent University. His research interests mainly concern numerical methods for electromagnetics, especially in electrical machines, modeling, and characterization of magnetic materials.

Rik Van de Walle (M'99) received the M.Sc. and Ph.D. degrees in engineering from Ghent University, Ghent, Belgium, in 1994 and 1998, respectively. After a visiting scholarship at the University of Arizona, Tucson, he returned to Ghent University. The topic of his Ph.D. and his work at the University of Arizona was medical imaging in general and, more specifically, the reconstruction of magnetic resonance images (MRI).

In 2001, he became a Professor in the Department of Electronics and Information Systems, Ghent University, and founded the Multimedia Lab. He has been involved in the organization of and/or review of papers for several international conferences and journals. His current research interests include multimedia content delivery, presentation and archiving, coding and description of multimedia data, content adaptation, interactive (mobile) multimedia applications, interactive digital TV. Multimedia Lab is one of the partners of the Interdisciplinary Institute for Broadband Technology (IBBT), which was founded by the Flemish Government in 2004.